Two novel colorimetric fluorescent probes: Hg²⁺ and Al³⁺ in the visual colorimetric recognition environment†

Wenxia Zhong,[a] Lizhen Wang, ![ID][b] Shimin Fang,[a] Dawei Qin,[a] Jianhua Zhou,[a] Geng Yang[a] and Hongdong Duan ![ID]*[a]

Two new dual channel Schiff base fluorescent probes, **Tri-R6G** and **Tri-Flu**, were synthesized, and can detect Hg²⁺ and Al³⁺, respectively. The two probes were characterized by FTIR, ¹H NMR, ¹³C NMR and HRMS, and their optical properties were detected by UV and FL. Test results showed the probes' detection of Hg²⁺ and Al³⁺ compared to other metal ions (Ag⁺, Co²⁺, Cd²⁺, Mg²⁺, Cu²⁺, Ni²⁺, Ba²⁺, Pb²⁺, Cr³⁺, Al³⁺, Zn²⁺, Hg²⁺, K⁺, Ga²⁺ and Fe³⁺), respectively. Besides, the detection limits were determined to be 1.61×10^{-8} M and 1.15×10^{-8} M through the standard curve plot, respectively. The photoelectron transfer (PET) mechanism was guessed by the Job's plot and the infrared titration. Corresponding orbital electron distribution and molecular geometry configurations of the compounds were predicted by density functional theory (DFT). In addition, the prepared test paper changed from white to pink when the target ion was detected. The color changed from colorless to pink in a solution having a concentration of 10^{-5} M.

1. Introduction

With the rapid development of industries, metal ion pollution has become a serious environmental problem.[1–6] Mercury is the only metal that exists as a liquid state, and at room temperature, mercury can evaporate into the highly toxic mercury vapor.[7–13] Even worse is that mercury can be enriched by passive plants and converted into more toxic organic mercury through biotransformation, which can easily enter the human body and cause various toxic effects in the human body. For example, prolonged exposure to high concentrations of mercury usually causes brain damage and death.[14–16] The latest statistics revealed that the amount of mercury ingested by a human had reached 20–30 μg d⁻¹, and in heavily polluted areas, it was as high as 200–300 μg d⁻¹ which poses serious threats to human health.[17,18] Therefore, the prevention and control of mercury pollution has become an urgent problem to be solved for countries all over the world. On the other hand, aluminum is an amphoteric element that reacts with both acids and alkalis.[19–27] Compounds formed after the reaction are easily absorbed by the intestines and can enter the brain, thus affecting the mental development of children and leading to senile dementia. Studies have shown that aluminum can cause decreased exercise and learning and memory, and affect children's mental development. Aluminum can also affect the reproductive capacity of male animals and inhibit fetal growth and development, and cause bone problems through interaction with calcium and phosphorus systematic damage and deformation, rickets, osteoporosis, *etc.* Consequently, the detection of aluminum is particularly important.[28–30]

Schiff base fluorescent probes have been widely used for detection of metal ions owing to their high sensitivity, low detection concentrations and perfect stability.[31–37] The C=N bond in Schiff fluorescent probes can form a stable complex with metal ions accompanied with an obvious fluorescence intensity enhancement or attenuation, which can be applied for detecting metal ions. Therefore, many Schiff base fluorescent probes have been developed for highly selective and sensitive detecting Hg²⁺ and Al³⁺.[38–44] For example, the Mahajan group[45] reported a novel pyridazine-oxime-based fluorescent probe that enhanced fluorescence recognition of Hg²⁺ at 550 nm in DMSO/H₂O (8/2, v/v) solution with a low detection limit (26.1 nM). This probe was further applied to detect Hg²⁺ in human cervical cancer HeLa cells, which indicated its potential applicable in biological samples. The Hou group[46] synthesized a turn-on fluorescent probe that could be complexed with Al³⁺ in a ratio of 1 : 1 to change the color of the solution from pale yellow to yellow. The detection limit of this probe was 82.2 nM and the fluorescence was significantly enhanced at 480 nm, which had potential application value in sensor development. However,

[a]School of Chemistry and Pharmaceutical Engineering, Qilu University of Technology (Shandong Academy of Sciences), Ji'nan, Shandong Province, China 250353. E-mail: hdduan67@163.com; Tel: +86 13153035598

[b]Biology Institute, Qilu University of Technology (Shandong Academy of Sciences), Ji'nan, Shandong Province, China 250014
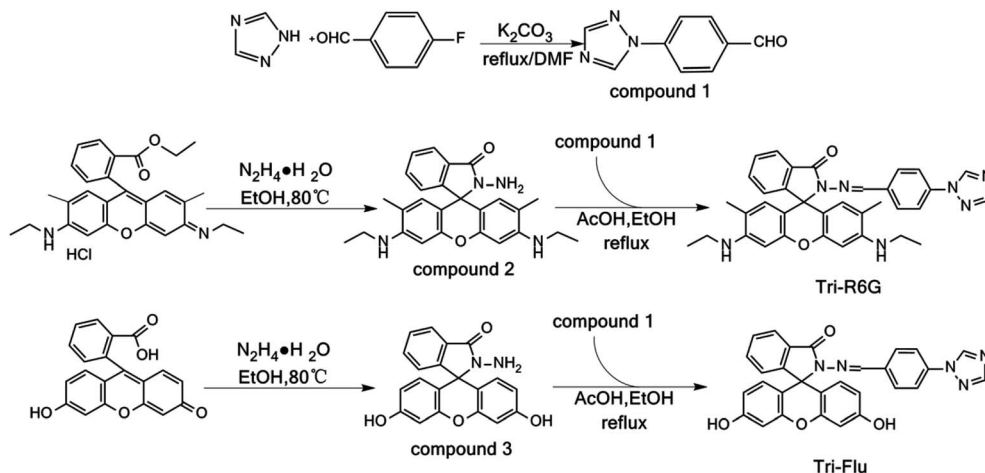
Scheme 1 Synthesis of probes **Tri-R6G** and **Tri-Flu**.

the above-mentioned fluorescent probes usually need tedious synthesis routines and are insensitive for detecting low concentration metal ions. Therefore, it is necessary to develop highly sensitive and selective fluorescent probes for detection of Hg^{2+} and Al^{3+}.

Triazole, a nitrogen-containing heterocyclic compound having unique biological activities, low toxicity and high systemicity,[47–51] has been widely used as key intermediates in the synthesis of various pesticides or pharmaceutical. Neupane group[52] reported a triazolyl complex based on a photoelectron transfer (PET) mechanism, which could detect Hg^{2+} under neutral and weakly acidic conditions with the detection limit of 672 nM. Chereddy group[53] synthesized a rhodamine-based fluorescent probe containing a 1,2,3-triazole ring under the guidance of soft and hard acid–base theory. It had 1 : 1 binding with Cu^{2+} and the detection limit was 60 nM, which could be used to detect Cu^{2+} biological samples. Two novel Schiff base fluorescent probes are synthesized, by grafting triazole on Rhodamine 6G and fluorescein derivatives, triazolyl benzaldehyde, Rhodamine 6G internal hydrazide Schiff base and triazolyl benzaldehyde fluorescein acyl hydrazide Schiff base (**Tri-R6G** and **Tri-Flu**).The structures of **Tri-R6G** and **Tri-Flu** were confirmed by FTIR, ^{1}H NMR, ^{13}C NMR and HRMS, and they were detected Hg^{2+} and Al^{3+} by UV and FL. The sensitive detection limits of these two probes were 1.61×10^{-8} M and 1.15×10^{-8} M, respectively. In addition, we used the probe to prepare the test paper, the prepared test paper changed from white to pink when the target ion was detected. The PET mechanism was guessed by Job's plot and infrared titration plot and was supported by theoretical calculations (Scheme 1).

2. Experimental section

2.1 General procedure

The solvents and drugs used in the experiments were all analytical grade and obtained from commercial sources. (1,2,4-Triazole, Rhodamine 6G and Fluorescein were purchased from

Aladdin). The ^{1}H NMR (400 MHz) and ^{13}C NMR (100 MHz) spectra were measured on a Bruker AV-400 spectrometer with DMSO-d_6 used as the solvent and tetramethylsilane (TMS) as the internal standard. Infrared measurements were performed using a KBr pellet technique on a Bruker ALPHA FT-IR spectrometer in the 4000–400 cm^{-1} region. High resolution mass spectrometry (HRMS) was performed using an Agilent 6510 precision mass Q-TOF LC/MS system. Fluorescence spectra were recorded on a Hitachi Fl-4600 fluorescence spectrophotometer with a scan rate of 2400 nm min^{-1}. Ultraviolet-visible (UV-vis) absorption were measured on SHIMADZU UV-2600.All experiments were performed at room temperature.

2.2 Synthesis

2.2.1 Synthesis of compound 1.[31] All glassware were cleaned with freshly lye, subsequently rinsed with copious amount of distilled water, and dried well before use. In a typical experiment, in a 250 mL three-necked, round-bottomed flask, was added 1.40 g of 1,2,4-triazole (20.19 mmol), 2.48 g of p-fluorobenzaldehyde (19.96 mmol), and 3.09 g of anhydrous potassium carbonate (22.39 mmol) dissolved in 100 mL of DMF, the reaction was allowed to proceed under vigorous stirring at 100 °C. After 24 hours, the reaction was cooled to 25 °C and poured into 300 mL of ice-water. Some buff solids precipitated, which was subjected to filtration, and the filtrate was recrystallized with ethyl acetate and dried in vacuum to give compound **1** as a white solid (2.69 g, yield 91%).

Triazole benzaldehyde (compound 1). IR (KBr): 1689, 1604, 1519, 1207, 981, 837 cm^{-1}; ^{1}H NMR (DMSO-d_6, 400 MHz): δ 10.02 (s, 1H), 8.45 (s, 1H), 8.04 (d, J = 8.5 Hz, 2H), 7.92 (d, J = 8.8 Hz, 2H), 7.16 (s, 1H); ^{13}C NMR (DMSO-d_6, 100 MHz): δ 165.91, 158.65, 152.86, 133.04, 129.80, 128.85, 123.87, 122.80, 112.44, 110.40, 102.81, 65.07, 56.48, 40.61, 40.19; ESI-TOF HRMS (m/z): calcd for $C_9H_7N_3O$, $[M + H]^+$, 174.1405; found, 173.1715.

2.2.2 Synthesis of compound 2. Rhodamine 6G (5.06 g, 10.56 mmol) and hydrazine (1.78 g, 35 mmol) were placed in a flask, and anhydrous ethanol was added as a solvent. The

reaction mixture was allowed to warm 78 °C under a refluxing device and stirred at ambient temperature for 4 hours, a solid precipitated was formed. The mixture was filtered and the filtrate was washed with hot ethanol and dried under vacuum to give compound **2** as a colorless solid (4.85 g, yield 79%).

Rhodamine 6G hydrazide (compound 2). IR (KBr): 3417, 3101, 2966, 1714, 1622, 1519, 1467, 1276 cm^{-1}; ^{1}H NMR (DMSO-d_6, 400 MHz): δ 7.77–7.73 (m, 1H), 7.49–7.42 (m, 2H), 6.95–6.90 (m, 1H), 6.26 (s, 2H), 6.10 (s, 2H), 4.99 (t, J = 5.3 Hz, 2H), 4.21 (s, 2H), 3.13 (p, J = 6.8 Hz, 4H), 1.88 (d, J = 9.9 Hz, 6H), 1.21 (t, J = 7.0 Hz, 6H); ^{13}C NMR (DMSO-d_6, 100 MHz): δ 165.18, 152.05, 151.31, 147.34, 132.23, 129.45, 127.97, 126.96, 123.40, 122.11, 117.77, 104.95, 95.86, 64.99, 37.44, 17.03, 14.13; ESI-TOF HRMS (m/z): calcd for $C_{26}H_{28}N_4O_2$, $[M + H]^+$, 429.2375; found, 428.2212.

2.2.3   Synthesis of compound 3.[54] Fluorescein (4.89 g, 14.69 mmol) and hydrazine (1.24 g, 24.77 mmol) were placed in a flask, and anhydrous ethanol was added as a solvent. The reaction mixture was heated to 78 °C and stirred at ambient temperature for 5 hours. The reaction was cooled to 25 °C and poured into 300 mL of ice water to give a white solid. The mixture was filtered and the filtrate was washed with ice-water

and dried under vacuum to give compound **3** as a yellow solid (4.03 g, yield 66%).

Fluorescein endonyl hydrazide (compound 3). IR (KBr): 3439, 3121, 2805, 1713, 1689, 1609, 1587, 1217 cm^{-1}; ^{1}H NMR (DMSO-d_6, 400 MHz): δ 9.62 (s, 2H), 7.79 (m, 1H), 7.45–7.52 (m, 2H), 6.97 (m, 1H), 6.58–6.59 (d, J = 2.4 Hz, 2H), 6.38–6.47 (m, 4H), 4.37 (s, 2H); ^{13}C NMR (DMSO-d_6, 100 MHz): δ 192.54, 153.47, 143.59, 141.19, 135.45, 131.74, 119.95, 56.47, 19.01; ESI-TOF HRMS (m/z): calcd for $C_{20}H_{14}N_2O_4$, $[M + H]^+$, 347.1161; found, 346.0954.

2.2.4   Synthesis of Tri-R6G. In a 250 mL three-necked, round-bottomed flask, was added 0.87 g of compound **1** (50.28 mmol), 2.23 g of compound **2** (52.10 mmol) and glacial acetic acid dissolved in 100 mL of DMF, the reaction was allowed to proceed under vigorous stirring at 100 °C. After 5 hours, 200 mL of ice water was added and some pink solids precipitated. The solid was resuspended with acetone, crystallized and dried under vacuum to give **Tri-R6G** as a pink solid (2.05 g, yield 66%).

Tri-R6G. IR (KBr): 3421, 2976, 1689, 1611, 1502, 1368, 1146 cm^{-1}; ^{1}H NMR (DMSO-d_6, 400 MHz): δ 9.30 (s, 1H), 8.76 (s, 1H), 8.24 (s, 1H), 7.92 (d, J = 7.2 Hz, 1H), 7.86 (d, J = 8.6 Hz, 2H), 7.64–7.54 (m, 4H), 7.06 (d, J = 7.3 Hz, 1H), 6.34 (s, 2H), 6.18 (s,
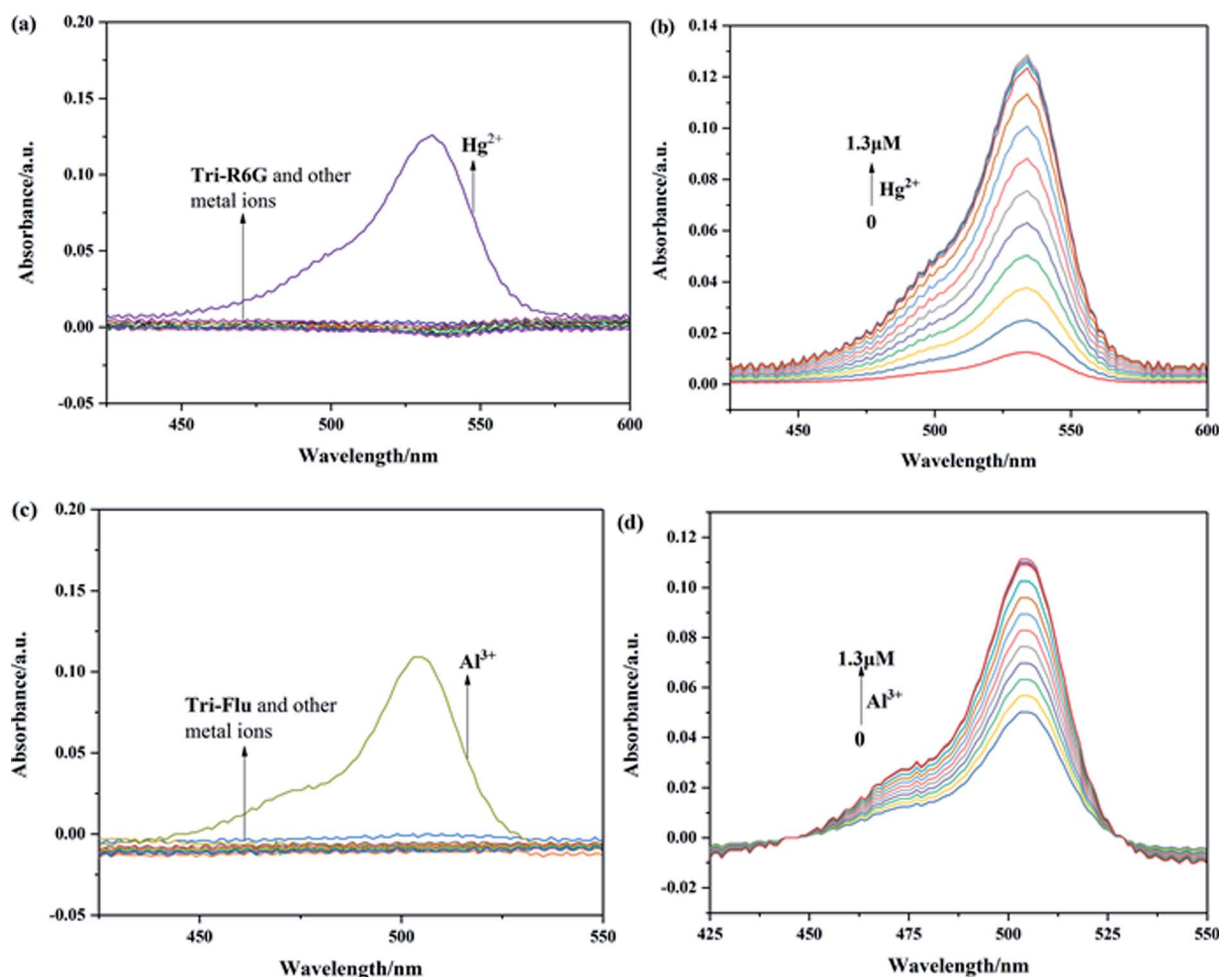

Fig. 1 UV-visible absorption of **Tri-R6G** (a) and **Tri-Flu** (c) in the presence and absence of different metal ions in a mixed solution of DMSO/H$_2$O (7/3, v/v) at 25 °C. (b) and (d) Upon titration with Hg^{2+} and Al^{3+} (1 × 10^{-5} M, 0–1.3 μM), respectively.

2H), 5.07 (t, $J = 5.3$ Hz, 2H), 3.18–3.09 (m, 4H), 1.85 (d, $J = 9.1$ Hz, 6H), 1.20 (t, $J = 7.1$ Hz, 6H); ^{13}C NMR (DMSO-d_6, 100 MHz): δ 163.76, 152.52, 151.06, 147.80, 142.38, 137.54, 133.92, 128.74, 127.95, 126.84, 123.81, 123.02, 119.55, 118.22, 105.06, 95.75, 37.43, 16.94, 14.11; ESI-TOF HRMS (m/z): calcd for $C_{35}H_{33}N_7O_2$, $[M + H]^+$, 584.2752; found, 583.2696.

2.2.5 Synthesis of Tri-Flu. In a 250 mL three-necked, round-bottomed flask, was added 0.18 g of compound **1** (1.04 mmol), 0.52 g of compound **3** (1.21 mmol) and glacial acetic acid dissolved in 100 mL of ethanol, the reaction was allowed to proceed under vigorous stirring at 78 °C. After 5 hours, 200 mL of ice water was added and some buff solids precipitated. The solid was resuspended with acetone, crystallized and dried under vacuum to give **Tri-Flu** as a buff solid (0.44 g, yield 63%).

Tri-Flu. IR (KBr): 3427, 3120, 1697, 1613, 1509, 1450, 1315 cm^{-1}; ^1H NMR (DMSO-d_6, 400 MHz): δ 9.93 (s, 2H), 9.31 (s, 1H), 9.13 (s, 1H), 8.25 (s, 1H), 7.94 (d, $J = 7.3$ Hz, 1H), 7.87 (d, $J = 8.5$ Hz, 2H), 7.62 (dd, $J = 14.4, 6.6$ Hz, 4H), 7.16 (d, $J = 7.4$ Hz, 1H), 6.67 (d, $J = 2.0$ Hz, 2H), 6.49 (dd, $J = 18.9, 9.6$ Hz, 4H); ^{13}C NMR (DMSO-d_6, 100 MHz): δ 163.63, 158.57, 152.31, 150.18, 128.02, 119.54, 112.30, 110.21, 102.45, 55.98, 18.51; ESI-TOF HRMS (m/z): calcd for $C_{29}H_{19}N_5O_4$, $[M + H]^+$, 502.1501; found, 501.1437.

3. Results and discussion

3.1 UV-vis absorption spectra

The recognition abilities of probes **Tri-R6G** and **Tri-Flu** were investigated in a mixed solution of DMSO/H_2O (7/3, v/v, 10 μM) in the presence and absence of different metal ions including Ag^+, Co^{2+}, Cd^{2+}, Mg^{2+}, Cu^{2+}, Ni^{2+}, Ba^{2+}, Pb^{2+}, Cr^{3+}, Al^{3+}, Zn^{2+}, Hg^{2+}, K^+, Ga^{2+} and Fe^{3+}. As shown in Fig. 1(a), the absorption spectrum of **Tri-R6G** in the solution of DMSO/H_2O (7/3, v/v, 10 μM) exhibited a low energy band centered at 534 nm. The addition of Hg^{2+} resulted in an obvious color change from colorless to pink, whereas adding other metal ions could not lead to any color changes. In Fig. 1(b), the intensity of the absorption band at 534 nm increased distinctly upon gradual addition of Hg^{2+} (0–1.3 μM). The transparent solution of **Tri-**

R6G changed to pink instantly after addition of Hg^{2+} ion. These results proved probe **Tri-R6G** exhibited high selectivity toward Hg^{2+} on the UV-vis spectrum. The absorption band appeared at 534 nm might be caused by the ring opening of the lactam. Similarly, the UV-vis absorption of probe **Tri-Flu** also showed two bands as shown in Fig. 1(c), a weak energy band at 504 nm. In Fig. 1(d), the intensity of the absorption band at 504 nm increased distinctly upon gradual addition of Al^{3+} (0–1.3 equiv.). The transparent solution of **Tri-Flu** changed to pink instantly after addition of Al^{3+} ion. Compared with other metal ions, the addition of Al^{3+} resulted in an obvious color change from colorless to pink, which proved the high selectivity of probe **Tri-Flu** toward Al^{3+}.

3.2 Fluorescence spectra

To investigate the optical properties of probes **Tri-R6G** and **Tri-Flu**, their fluorescence spectra toward various metal ions were explored in a mix solution of DMSO/H_2O (10 μM) as shown in Fig. 2. Free sensor **Tri-R6G** showed a weak absorption band at 560 nm, whereas that of sensor **Tri-Flu** was at 541 nm. After addition of Hg^{2+}, the solution of probe **Tri-R6G** showed an obvious and strong absorption band at 560 nm (Fig. 2(a)), while addition of other metal ions elicited no or weak fluorescence enhancement that could be ignored. These results revealed again the high selectivity and specificity of probe **Tri-R6G** against Hg^{2+}. In addition, with Rhodamine 6G as the reference material, the relative fluorescence quantum yield of probe **Tri-R6G** is 0.1089 $(Y_f = k_f/(k_f + \Sigma k_i))$. The similar results were observed in the fluorescence spectra of **Tri-Flu** (Fig. 2(b)), which exhibited high selectivity toward Al^{3+} compared with various other metal ions added to the solution. When probes **Tri-R6G** and **Tri-Flu** bind to metal ions Hg^{2+} and Al^{3+}, their fluorescence intensity is steady, and no obvious attenuation within half an hour (Fig. 3(a) and (b)). Therefore, probe **Tri-R6G** and **Tri-Flu** can be used to detect Hg^{2+} and Al^{3+}, respectively.

The sensitivities of probes **Tri-R6G** toward Hg^{2+} and **Tri-Flu** toward Al^{3+} were investigated through fluorescence titration experiments as described in Fig. 4. With the concentration of Hg^{2+} added to the solution increasing, fluorescence spectra of
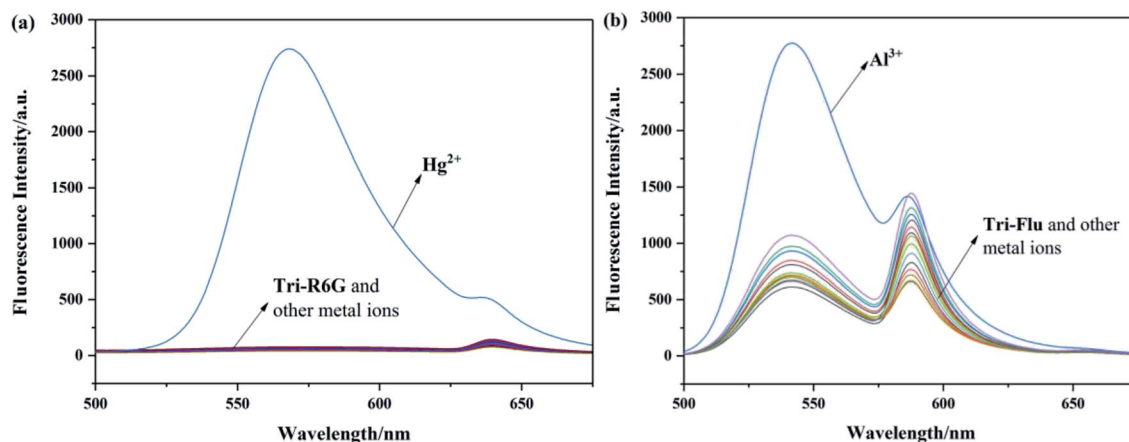

Fig. 2 The fluorescence spectra of **Tri-R6G** (a) (10 μM) and **Tri-Flu** (b) (10 μM) in the presence and absence of different metal ions (10 μM) in DMSO/H_2O (7/3, v/v), respectively.
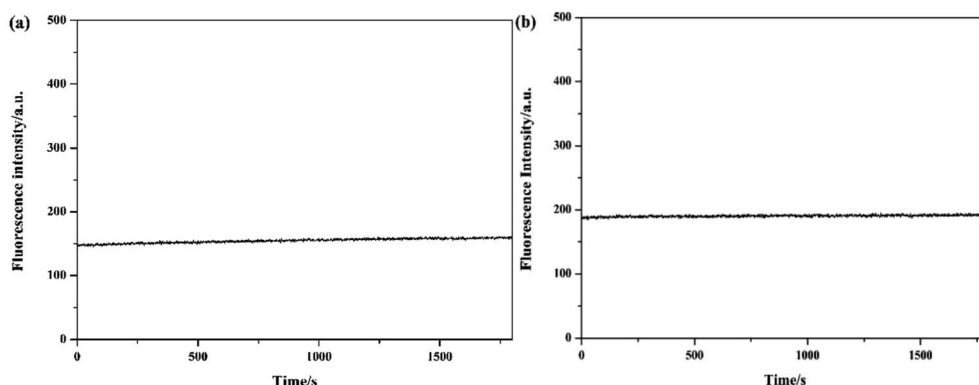
Fig. 3   The photo stability experiments of probes Tri-R6G (a) and Tri-Flu (b).
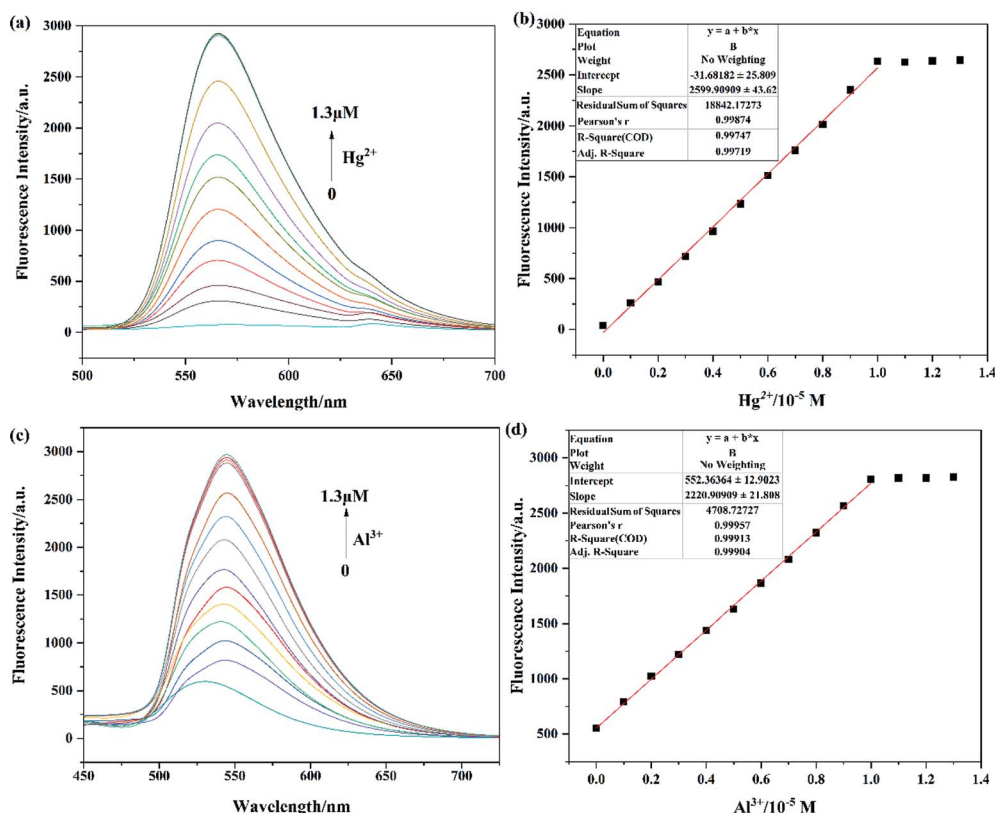

Fig. 4   The fluorescence spectra of Tri-R6G (a) and Tri-Flu (c) (10 μM) with the increasing concentration of Hg^{2+} and Al^{3+} ions (0–1.3 μM) in DMSO/H_2O (7/3, v/v) and ethanol, respectively; the linear fit between Tri-R6G (b) with Hg^{2+} ions and Tri-Flu (d) with Al^{3+} ions.

probe Tri-R6G showed significant enhancement (Fig. 4(a)), which could be ascribed to the coordination reaction of Tri-R6G with Hg^{2+} and consequently decreased the PET process and C=N isomerization. In addition, there is a good linear relationship ($R_1 = 0.99874$) between fluorescence intensity and Hg^{2+} concentration (Fig. 4(b)). The fluorescence titration experiment of Tri-Flu toward Al^{3+} was also carried out as shown in Fig. 4(c). With the increase of Al^{3+} concentration, the fluorescence intensity of Tri-Flu increased significantly and showed a good linear relationship (Fig. 4(d), $R_2 = 0.99957$).

Furthermore, according to the formula $DL = 3\sigma/k$, the detection limit of Tri-R6G toward Hg^{2+} was calculated to be 1.61×10^{-8} M, and that of Tri-Flu toward Al^{3+} was 1.15×10^{-8} M. These results demonstrated the high sensitivity of the synthetic probes and their potential application for the detection of Hg^{2+} and Al^{3+}.

When more than 1 equiv. of Hg^{2+} was added, no change in the fluorescence intensity was observed. This result might prove that the binding stoichiometry of Tri-R6G to Hg^{2+} was 1 : 1. Therefore, a drawing experiment of Job was performed to study
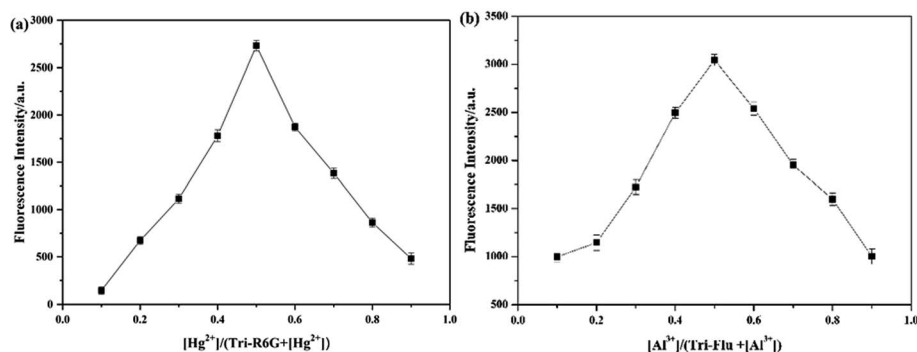
Fig. 5 Job's plot for determining the stoichiometry of **Tri-R6G** + Hg^{2+} (a) in $DMSO/H_2O$ (7/3, v/v) solution and **Tri-Flu** + Al^{3+} (b) in ethanol solution.
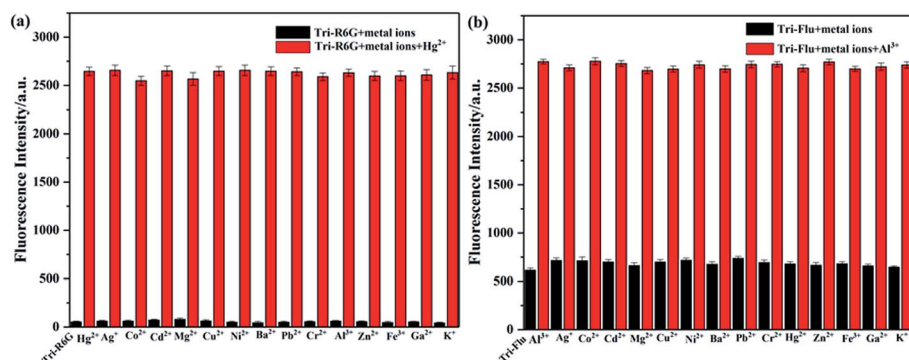

Fig. 6 The black bars represent the fluorescent intensity of sensor **Tri-R6G** (a) or **Tri-Flu** (b) and various metal ions (1.0 equiv.) in solution; the red bars represent the fluorescent intensity of sensor **Tri-R6G** + Hg^{2+} (a) or **Tri-Flu** + Al^{3+} (b) (1.0 equiv.) in solution.

the combined stoichiometry between the probes and the metal ions. As shown in Fig. 5(a), the maximum fluorescence intensity of a mole fraction of about 10^{-5} M was measured, and it is shown that a complex is formed between **Tri-R6G** and Hg^{2+} in a mole ratio of 1 : 1. Similarly, the formation of a complex between **Tri-Flu** and Al^{3+} in a ratio of 1 : 1 can be observed in Fig. 5(b).

3.3 Competition experiments

High selectivity is an important parameter for studying the performance of fluorescent probes. Therefore, the competition experiment was carried out to examine the binding ability of synthetic probes toward metal ions in a mix solution of DMSO and H_2O, and the metal concentrations used in this experiment were all 10^{-5} M. As shown in Fig. 6(a), addition of Hg^{2+} to
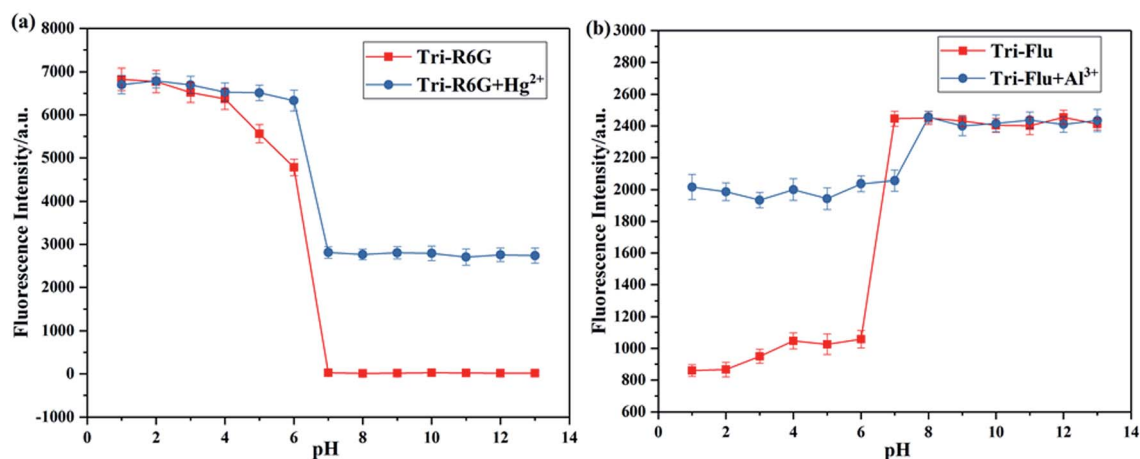

Fig. 7 Fluorescence response of sensor **Tri-R6G** (a) and **Tri-Flu** (b) (10 μM) as a function of pH (pH 1.0–13.0) in the absence and presence of Hg^{2+} and Al^{3+} (10 μM), receptively, at room temperature.
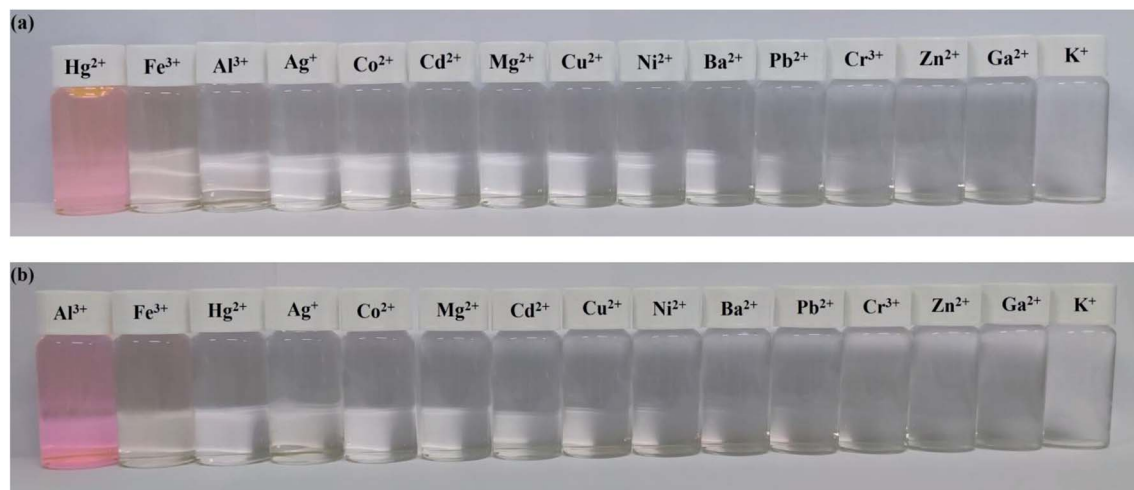
Fig. 8 Colorimetric performance of sensor **Tri-Flu** + Hg^{2+} (a) (10 μM) and **Tri-R6G** + Al^{3+} (b) (10 μM) upon addition of different metal ions (1.0 μM) in DMSO/H_2O (7/3, v/v) solution and ethanol solution.

a solution of **Tri-R6G** leaded to a mixture with obvious fluorescence enhancement, which could not affect by adding other metal ions to the mixture, indicating the high selectivity of probe **Tri-R6G**. Similar experiments depicted Fig. 6(b) also proved the high selectivity of probe **Tri-Flu** toward Al^{3+}.

3.4 pH effects

It has been well proved that pH value is essential for the detection ability of fluorescent probes. Hence, the effect of pH on fluorescence intensity was investigated to evaluate the potential applicability of probes **Tri-R6G** and **Tri-Flu** as shown in Fig. 7. Clearly, the fluorescence intensity of probe **Tri-R6G** significantly reduced with the increase of pH when it was below 6, whereas the fluorescence intensity was observed to be held steady between pH 7–13, when Hg^{2+} was added, the probe also had strong fluorescence intensity at pH 7 or higher. Which proved that probe **Tri-R6G** could test Hg^{2+} within a biological scale of pH values. Oppositely, the fluorescence intensity of probe **Tri-Flu** significantly increased with the increase of pH when it was above 6, but at high pH value (>7), the fluorescence intensity tends to saturation. When Al^{3+} was added, the probe also had strong fluorescence intensity when the pH is below 7. Which indicated that **Tri-Flu** can be used in acidic environments.

3.5 Colorimetric experiment

The specificity of probes **Tri-R6G** and **Tri-Flu** toward Hg^{2+} and Al^{3+} were also investigated by colorimetric experiments, respectively. As shown in Fig. 8(a), addition of the same concentration of Hg^{2+} was to a solution of sensor **Tri-R6G** in DMSO/H_2O (7/3, v/v, 10 μM) caused obvious color change from colorless to pink and the whole process was finished only in one second, suggesting that sensor **Tri-R6G** could be used for naked-eye recognition of Hg^{2+} with concentration as low as 10 μM. While, the addition of other metal ions showed almost no color changes in absorption peak, which demonstrated the high

specificity of probe **Tri-R6G** for detecting Hg^{2+}. Similarly, an obvious color change from colorless to pink was observed after addition of the same concentration of Al^{3+} to a solution of **Tri-Flu** in DMSO/H_2O (7/3, v/v, 10 μM) as shown in Fig. 8(b), the same sensor showed no obvious color changes in the presence of other metal ions. These results proved that probe **Tri-Flu** could be employed as a high sensitivity sensor for naked eye recognition of Al^{3+}.

In order to study the practical application of probes **Tri-R6G** and **Tri-Flu**, we dipped the filter paper into a solution of **Tri-R6G** or **Tri-Flu**, and then dried in the air. Subsequently, the test strip was treated with Hg^{2+} or Al^{3+} solution (mM) which resulted in an obvious color change from colorless to light pink. Therefore, the test strips could be conveniently utilized for detecting Hg^{2+} and Al^{3+} in solutions (Fig. 9).

We compare the water in the river with the water without Hg^{2+}. As shown in Fig. 10(a), the water in the river is added to
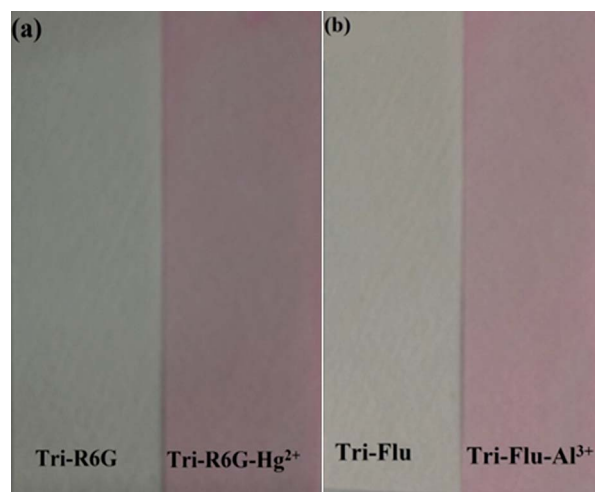

Fig. 9 Photographs showing the color changes of sensor **Tri-R6G** (a) and **Tri-Flu** (b) before and after addition of Hg^{2+} and Al^{3+} under sunlight, respectively.
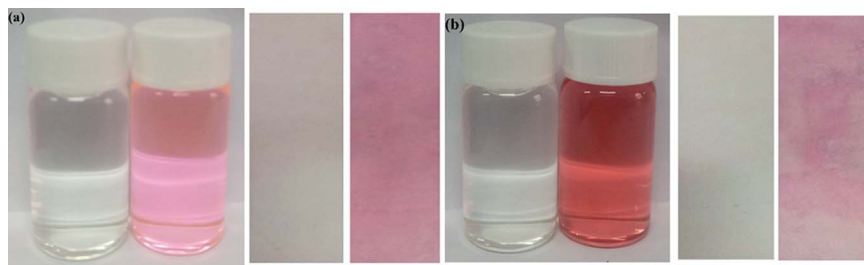
Fig. 10 (a) Photographs showing the color change of the sensor **Tri-R6G** solution and test strips in a water sample containing no Hg^{2+} and water samples in the river. (b) Photographs showing the color change of the sensor **Tri-Flu** solution and test strips in a water sample containing no Al^{3+} and water samples in the river.
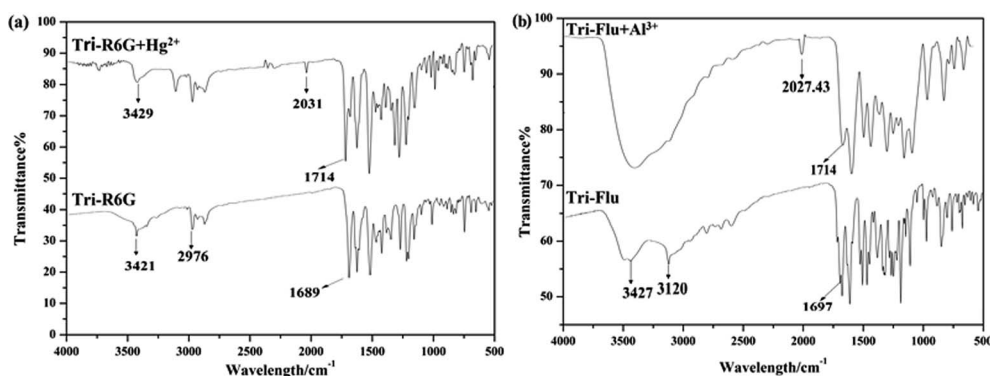

Fig. 11 The FT-IR spectrum of **Tri-R6G** and **Tri-R6G** + Hg^{2+} (a); the FT-IR spectrum of **Tri-Flu** and **Tri-Flu** + Al^{3+} (b).

the **Tri-R6G** probe solution. The color changes from colorless to pink, prepared by **Tri-R6G**. The test strip turns pink. Similarly, as shown in Fig. 10(b), probe **Tri-Flu** has same phenomenon with**Tri-R6G**. These results demonstrate that the probe **Tri-R6G** has great promise to determine Hg^{2+} in a simple, convenient and portable way. Similarly, the same is true for probe **Tri-Flu**.

3.6 Binding sites

The FT-IR spectrum of probe **Tri-R6G** and complex **Tri-R6G** + Hg^{2+} were shown in Fig. 11(a). Free probe **Tri-R6G** showed stretching vibration bands assignable to N–H and C=N at 3429 and 1689 cm^{-1}, respectively. While complexation of **Tri-R6G** with Hg^{2+} resulted in the obvious shift of N–H stretching vibration band from 3429 cm^{-1} to 3421 cm^{-1}, and the tretching vibration band of C=N shifted to 1714 cm^{-1}. Similarly, the IR spectrum of probe **Tri-Flu** and **Tri-Flu** + Al^{3+} were shown in Fig. 11(b). Free probe **Tri-Flu** showed stretching vibration bands assignable to O–H and C=N at 3427 and 1697 cm^{-1}, respectively. When Al^{3+} is added, the stretching vibration band of C=N shifted to 1714 cm^{-1}.

To further study the binding interactions of sensor **Tri-R6G** + Hg^{2+} and **Tri-Flu** + Al^{3+}, ^1H NMR titrations have been performed in DMSO-d_6 as shown in Fig. 12. As shown in Fig. 12(a), upon addition of Hg^{2+} (1.0 μM) to the solution of sensor **Tri-R6G**, the H proton signals of C=N and –NH_2 at 9.30, 8.75 and 8.24, respectively. But, after the addition of Hg^{2+} (1.0 μM) to the solution of sensor **Tri-R6G**, the H proton signals of C=N and

–NH_2 shifted to higher δ values (9.43, 8.79 and 8.36 ppm) with respect to sensor **Tri-Flu**. Under the same conditions, upon addition of Al^{3+} (1.0 μM) to the solution of sensor **Tri-Flu**, the H proton signal of phenolic O–H located and H proton signal of aldimine C=N shifted from δ 9.93 and 9.12 ppm to 9.96 and 9.14 ppm, respectively. To further study the binding interactions of sensor **Tri-R6G** + Hg^{2+} and **Tri-Flu** + Al^{3+}, ^{13}C NMR titrations have been performed in DMSO-d_6 as shown in Fig. 13. In the Fig. 13(a), after the addition of Hg^{2+} (1.0 μM) to the solution of sensor **Tri-R6G**, the C proton signals of C=N from 62 ppm to 48 ppm. Similarly, the addition of Al^{3+} (1.0 μM) to the solution of sensor **Tri-Flu**, the C proton signals of C=N from 56 ppm to 47 ppm in the Fig. 13(b). These data strongly draw the conclusion that when the probe binds with metal ions, the complexation reaction occurs at C=N position, which leads to the migration of intramolecular electrons and the H proton signals of C=N, –OH and –NH_2 generated offset, and the C proton signal of C=N is shifted.

Based on Job's plot and FT-IR, we predict the possible binding mechanism of probes with metal ions as shown in Scheme 2.[55–57] For free probe **Tri-R6G**, the photoelectron transfer (PET) process leads to the fluorescence quenching of rhodamine. Before the metal ions are bound, the sensor molecules appear to be fluorescently quenched. When the rhodamine hydrazide group is combined with the metal ion, the electron donating ability of the rhodamine hydrazide group is reduced, and the PET process is suppressed. The electrons
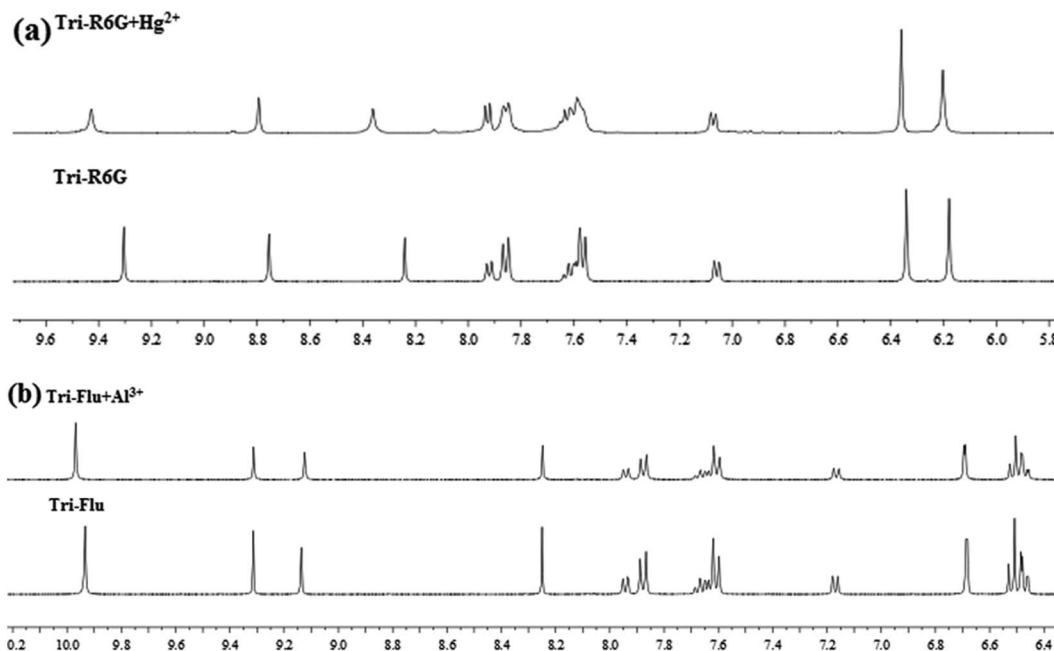
Fig. 12 The ^{1}H NMR of **Tri-R6G** and **Tri-R6G** + Hg^{2+} (a); the ^{1}H NMR spectrum of **Tri-Flu** and **Tri-Flu** + Al^{3+} (b).
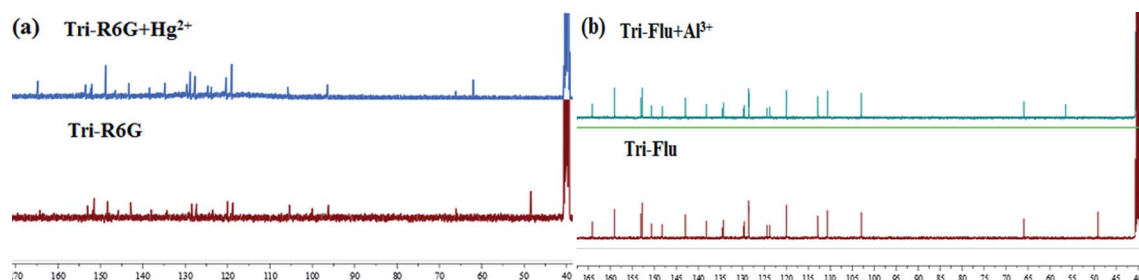

Fig. 13 The ^{13}C NMR of **Tri-R6G** and **Tri-R6G** + Hg^{2+} (a); the ^{13}C NMR spectrum of **Tri-Flu** and **Tri-Flu** + Al^{3+} (b).

excited by light in the fluorescent group can directly jump back to the original ground state orbital, thereby enhanced fluorescence emission of the fluorophore. Addition of Hg^{2+} causes the ring opening of lactam and the blocking of the PET process described above. Similarly, the complications of Al^{3+} with **Tri-Flu** blocks the PET process in fluorescein matrix, thereby causing obvious fluorescence enhancement.

3.7 Theoretical calculation

The optimized molecular structure, molecular orbital distribution and excitation energies of the synthetic probes were calculated by Gaussian 09 program and the density functional theory (DFT) at B3LYP/6-311++g(d.p) level. The optimized structures of probe **Tri-R6G** and **Tri-Flu** were shown in Fig. 14. The energy level, orbital distribution and orbital energy were
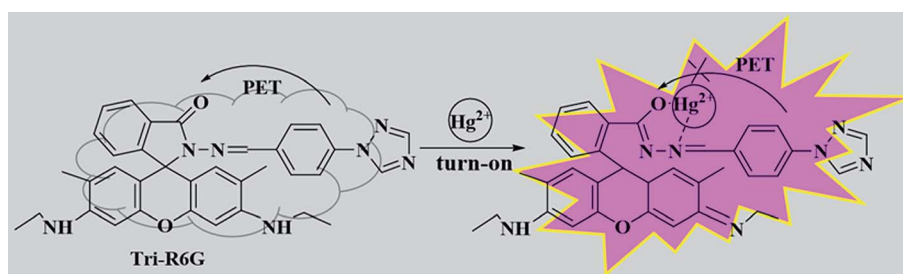
Scheme 2 The proposed sensing mechanism of sensor **Tri-R6G** and Hg^{2+}.
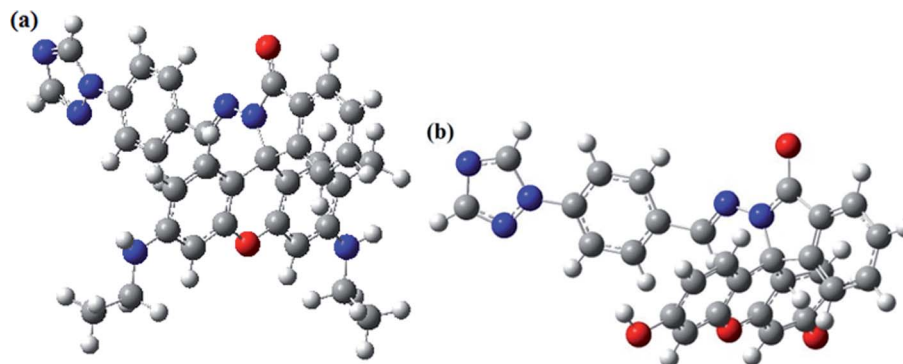
Fig. 14 The optimized molecular structures of **Tri-R6G** (a) and **Tri-Flu** (b).
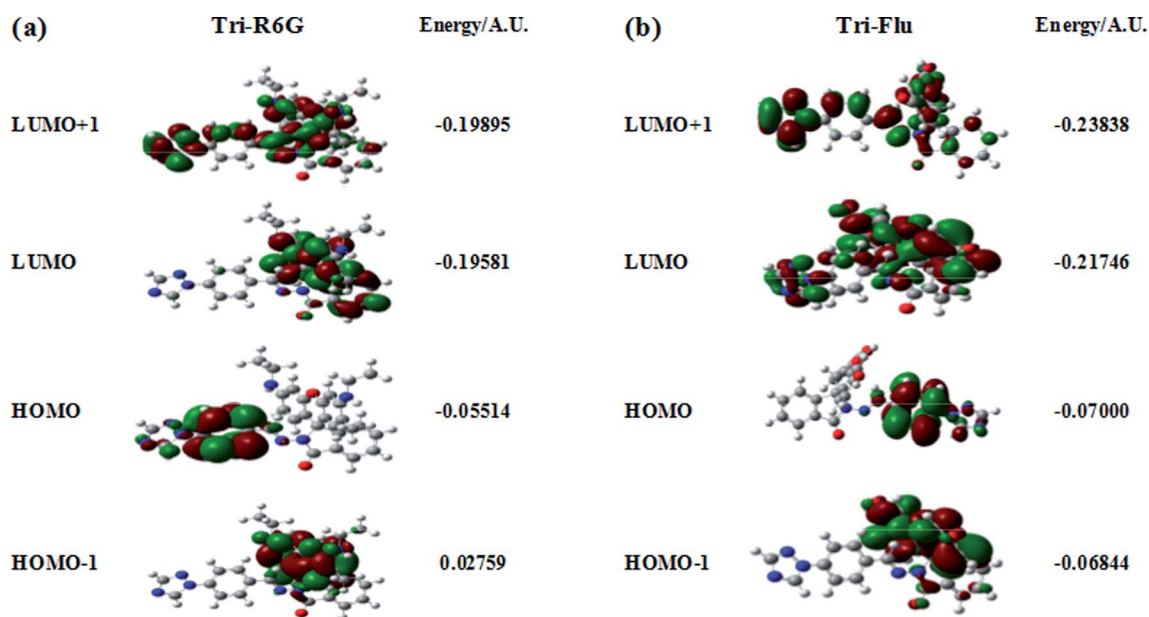

Fig. 15 Corresponding orbital electron distribution of probes **Tri-R6G** (a) and **Tri-Flu** (b).

listed in Fig. 15. The location of HOMO electron cloud of probe **Tri-R6G** is mainly at the benzene ring, as show in Fig. 15(a), theHOMO−1 and LUMO orbital electron clouds were populated on the Rhodamine 6G matrix, whereas the electron cloud of LUMO+1 almost delocalized over the whole structure. The overlap between them indicated that the electron transition could be easily implemented. The orbital energy of probe **Tri-R6G** increased in the order of HOMO−1 (0.02759), HOMO (−0.05514), LUMO (−0.19581) and LUMO+1 (−0.19895) were sequentially increased, also the energies of HOMO, LUMO, LUMO+1 were negative. It could be predicted that probe **Tri-R6G** could easily combined with metal cations. Probe **Tri-Flu** has a simpler electronic transition than probe **Tri-R6G**. In Fig. 15(b), the electron clouds of HOMO−1 and HOMO were delocalized on the fluorescein matrix, and the electron clouds of LUMO and LOMO+1 were mainly located the entire structure. Similarly, the orbital energy of probe **Tri-Flu** increased in the order of HOMO−1 (−0.06844), HOMO (−0.07000), LUMO (−0.21746),

LUMO+1 (−0.23838) were sequentially increased and negative. It was predicted that probe **Tri-Flu** might readily bind to metal cations. We also calculated the orbital energy differential of probe **Tri-R6G** and **Tri-Flu** were small, the results are shown in Table 1, which means that the electrons can be easily transitioned.

Table 1 Orbital energy differential of **Tri-R6G** and **Tri-Flu**

Compound	$\Delta E_{H \to L}(AU)$	$E_{H \to L+1}(AU)$	$E_{H-1 \to L}(AU)$
Tri-R6G	0.14067	0.14381	0.16822
Tri-Flu	0.14746	0.16838	0.14902

4. Conclusion

In summary, two kinds of novel fluorescent probes were synthesized and proved to have high applicability, low detection

limit and easy-to-handle. The properties of the probes were predicted by theoretical calculation, and their UV-vis and fluorescence properties were also investigated and the results demonstrated that the probes have specificity for Hg^{2+} and Al^{3+} over other detected metal ions based on the PET mechanism, respectively. In addition, these two probes are extremely resistant to interference from other metal ions, and can visually detect metal ions from white to pink in solution or test paper.

Conflicts of interest

There are no conflicts to declare.

Acknowledgements

References

1 C. Leyval, K. Turnau and K. Haselwandter, *Mycorrhiza*, 1997, **7**, 139–153.

2 Z. Li, Z. Ma, T. J. van der Kuijp, Z. Yuan and L. Huang, *Sci. Total Environ.*, 2014, **468**, 843–853.

3 T.-B. Chen, Y.-M. Zheng, M. Lei, Z.-C. Huang, H.-T. Wu, H. Chen, K.-K. Fan, K. Yu, X. Wu and Q.-Z. Tian, *Chemosphere*, 2005, **60**, 542–551.

4 Z. Guixia, L. Jiaxing, R. Xuemei, C. Changlun and W. Xiangke, *Environ. Sci. Technol.*, 2011, **45**, 10454.

5 A. M. Burke, J. P. Hanrahan, D. A. Healy, J. R. Sodeau, J. D. Holmes and M. A. Morris, *J. Hazard. Mater.*, 2009, **164**, 229–234.

6 J. Li, X. Xiao, X. Xu, J. Lin, Y. Huang, Y. Xue, P. Jin, J. Zou and C. Tang, *Sci. Rep.*, 2013, **3**, 3208.

7 J.-S. Wu, I.-C. Hwang, K. S. Kim and J. S. Kim, *Org. Lett.*, 2007, **9**, 907–910.

8 C.-W. Liu, Y.-T. Hsieh, C.-C. Huang, Z.-H. Lin and H.-T. Chang, *Chem. Commun.*, 2008, 2242–2244.

9 Z. Xiaolin, X. Yi and Q. Xuhong, *Angew. Chem.*, 2008, **47**, 8025–8029.

10 C. Vimlesh and K. S. Kim, *Chem. Commun.*, 2011, **47**, 3942–3944.

11 W. Shi and H. Ma, *Chem. Commun.*, 2008, **16**, 1856.

12 K. Manoj, K. Naresh, B. Vandana, S. Hardev, S. Parduman Raj and K. Tandeep, *Org. Lett.*, 2011, **13**, 1422–1425.

13 M. So Youn, C. N. Ri, K. Young Hee and C. Suk-Kyu, *J. Org. Chem.*, 2004, **69**, 181–183.

14 M. Vahabzadeh and M. Balali-Mood, *Int. J. Occup. Environ. Med.*, 2016, **7**, 116–122.

15 T. Y. K. Chan, *Clin. Toxicol.*, 2011, **49**, 886–891.

16 S. Ekino, M. Susa, T. Ninomiya, K. Imamura and T. Kitamura, *J. Neurol. Sci.*, 2007, **262**, 131–144.

17 C. M. Association, *Can. Med. Assoc. J.*, 2017, **189**, E475.

18 J. S. Ahn, K. W. Kang, W. Y. Kang, H. M. Lim, S. Cho, J. D. Moon and W. J. Park, *J. Occup. Health*, 2018, **60**, 89–93.

19 Z. Gao, J. Wang, Z. Li, W. Yang, B. Wang, M. Hou, Y. He, Q. Liu, T. Mann and P. Yang, *Chem. Mater.*, 2011, **23**, 3509–3516.

20 K. S. Hoon, C. H. Seok, K. Joohoon, L. Suk Joong, Q. Duong Tuan and K. Jong Seung, *Org. Lett.*, 2010, **12**, 560–563.

21 G. Férey, M. Latroche, C. Serre, F. Millange, T. Loiseau and A. Percheron-Guégan, *Chem. Commun.*, 2003, **24**, 2976–2977.

22 A. Sahana, A. Banerjee, S. Lohar, B. Sarkar, S. K. Mukhopadhyay and D. Das, *Inorg. Chem.*, 2013, **52**, 3627–3633.

23 B. Y. Fang, C. Li, Y. Y. Song, F. Tan, Y. C. Cao and Y. D. Zhao, *Biosens. Bioelectron.*, 2017, **100**, 41–48.

24 P. Cardiano, C. Foti, F. Giacobello, O. Giuffrè and S. Sammartano, *Biophys. Chem.*, 2018, **234**, 42–50.

25 F. Wang, H. Duan, D. Xing and G. Yang, *J. Fluoresc.*, 2017, **27**, 1721–1727.

26 J. Afshani, A. Badiei, N. Lashgari and G. M. Ziarani, *RSC Adv.*, 2016, **6**, 5957–5964.

27 C. L. Losq, D. R. Neuville, P. Florian, G. S. Henderson and D. Massiot, *Geochim. Cosmochim. Acta*, 2014, **126**, 495–517.

28 M. A. Akeson, D. N. Munns and R. G. Burau, *Biochim. Biophys. Acta Biomembr.*, 1989, **986**, 33–40.

29 G. Kubal, A. B. Mason, P. J. Sadler, A. Tucker and R. C. Woodworth, *Biochem. J.*, 1992, **285**(pt 3), 711–714.

30 M. Deleers, J. P. Servais and E. Wülfert, *Biochim. Biophys. Acta Biomembr.*, 1985, **813**, 195–200.

31 J. Liu, X. Meng, H. Duan, T. Xu, Z. Ding, Y. Liu and L. Lucia, *Sens. Actuators B Chem.*, 2016, **227**, 296–303.

32 X. Wang, T. Xu and H. Duan, *Sens. Actuators B Chem.*, 2015, **214**, 138–143.

33 P. Wu, D. L. Ma, C. H. Leung, S. C. Yan, N. Zhu, R. Abagyan and C. M. Che, *Chem. Eur J.*, 2009, **15**, 13008–13021.

34 Q. Xiao, S. Huang, Y. Liu, F.-f. Tian and J.-c. Zhu, *J. Fluoresc.*, 2009, **19**, 317.

35 W. Fang, G. Zhang, J. Chen, L. Kong, L. Yang, H. Bi and J. Yang, *Sens. Actuators B Chem.*, 2016, **229**, 338–346.

36 W. Li, X. Tian, B. Huang, H. Li, X. Zhao, S. Gao, J. Zheng, X. Zhang, H. Zhou and Y. Tian, *Biosens. Bioelectron.*, 2016, **77**, 530–536.

37 J.-c. Qin, L. Fan and Z.-y. Yang, *Sens. Actuators B Chem.*, 2016, **228**, 156–161.

38 V. Bhalla, M. Kumar, P. R. Sharma and T. Kaur, *Dalton Trans.*, 2013, **42**, 15063–15068.

39 A. Jiménez-Sánchez, N. Farfán and R. Santillan, *Tetrahedron Lett.*, 2013, **54**, 5279–5283.

40 H.-r. Cheng and Y. Qian, *RSC Adv.*, 2015, **5**, 82887–82893.

41 J. Afshani, A. Badiei, M. Karimi, N. Lashgari and G. Mohammadi Ziarani, *Appl. Organomet. Chem.*, 2017, **31**, e3856.

42 J. Feng, L. X. Duan, Z. B. Shang, J. B. Chao, Y. Wang and W. J. Jin, *Spectrochim. Acta A Mol. Biomol. Spectrosc.*, 2018, **201**, 185–192.

43 V. K. Gupta, A. K. Singh and L. K. Kumawat, *Sens. Actuators B Chem.*, 2014, **195**, 98–108.

44 Y. W. Choi, G. J. Park, Y. J. Na, H. Y. Jo, S. A. Lee, G. R. You and C. Kim, *Sens. Actuators B Chem.*, 2014, **194**, 343–352.

45 D. Mahajan, N. Khairnar, B. Bondhopadhyay, S. K. Sahoo, A. Basu, J. Singh, N. Singh, R. Bendre and A. Kuwar, *New J. Chem.*, 2015, **39**, 3071–3076.

46 L. Hou, J. Feng, Y. Wang, C. Dong, S. Shuang and Y. Wang, *Sens. Actuators B Chem.*, 2017, **247**, 451–460.

47 S. G. Agalave, S. R. Maujan and V. S. Pore, *Chem. Asian J.*, 2011, **6**, 2696–2718.

48 G. Aromí, L. A. Barrios, O. Roubeau and P. Gamez, *Coord. Chem. Rev.*, 2011, **255**, 485–546.

49 H. Kim, S. Lee, J. Lee and J. Tae, *Org. Lett.*, 2010, **12**, 5342–5345.

50 L. N. Neupane, J. M. Kim, C. R. Lohani and K.-H. Lee, *J. Mater. Chem.*, 2012, **22**, 4003–4008.

51 S. P. Sau and P. J. Hrdlicka, *J. Org. Chem.*, 2011, **77**, 5–16.

52 L. N. Neupane, J. M. Kim, C. R. Lohani and K. H. Lee, *J. Mater. Chem.*, 2012, **22**, 4003–4008.

53 N. R. Chereddy, S. Thennarasu and A. B. Mandal, *Sens. Actuators B Chem.*, 2012, **171**, 294–301.

54 G. Yang, X. Meng, Z. Wang, S. Fang, F. Wang, L. Wang, H. Duan and A. Hao, *New J. Chem.*, 2018, **42**, 14630–14641.

55 S. Lee, B. Rao and Y. Son, *Sens. Actuators B Chem.*, 2014, **196**, 388–397.

56 K. S. Min, R. Manivannan and Y.-A. Son, *Sens. Actuators B Chem.*, 2018, **261**, 545–552.

57 Y. Yang, R. Shen, Y. Wang, F. Qiu, Y. Feng, X. Tang, D. Bai, G. Zhang, W. Liu, *et al.*, *Sens. Actuators B Chem.*, 2018, **225**, 3479–3487.